

Graph Backdoor

Zhaohan Xi[†] Ren Pang[†] Shouling Ji[‡] Ting Wang[†]

[†]Pennsylvania State University [‡]Zhejiang University and Ant Financial

Abstract

One intriguing property of deep neural networks (DNNs) is their inherent vulnerability to backdoor attacks – a trojaned model responds to trigger-embedded inputs in a highly predictable manner while functioning normally otherwise. Surprisingly, despite the plethora of prior work on DNNs for continuous data (e.g., images), little is known about the vulnerability of graph neural networks (GNNs) for discrete-structured data (e.g., graphs), which is highly concerning given their increasing use in security-sensitive domains.

To bridge this gap, we present GTA, the first backdoor attack on GNNs. Compared with prior work, GTA departs in significant ways: *graph-oriented* – it defines triggers as specific subgraphs, including both topological structures and descriptive features, entailing a large design spectrum for the adversary; *input-tailored* – it dynamically adapts triggers to individual graphs, thereby optimizing both attack effectiveness and evasiveness; *downstream model-agnostic* – it can be readily launched without knowledge regarding downstream models or fine-tuning strategies; and *attack-extensible* – it can be instantiated for both transductive (e.g., node classification) and inductive (e.g., graph classification) tasks, constituting severe threats for a range of security-critical applications (e.g., toxic chemical classification). Through extensive evaluation using benchmark datasets and state-of-the-art models, we demonstrate the effectiveness of GTA: for instance, on pre-trained, off-the-shelf GNNs, GTA attains over 99.2% attack success rate with merely less than 0.3% accuracy drop. We further provide analytical justification for its effectiveness and discuss potential countermeasures, pointing to several promising research directions.

1 Introduction

Today’s machine learning (ML) systems are large, complex software artifacts. Due to the ever-increasing system scale and training cost, it becomes not only tempting but also necessary to re-use pre-trained models in building ML systems. It was estimated that as of 2016, over 13.7% of ML-related repositories on GitHub use at least one pre-trained model [24]. On the upside, this “plug-and-play” paradigm significantly simplifies the development cycles of ML systems [46]. On the downside, as most pre-trained models are contributed by untrusted third parties (e.g., ModelZoo [5]), their lack of standardization or regulation entails profound security implications.

In particular, pre-trained models are exploitable to launch *backdoor* attacks [19, 32], one immense threat to the security

of ML systems. In such attacks, a trojaned model forces its host system to misbehave when certain pre-defined conditions (“triggers”) are present but function normally otherwise. Such attacks can result in consequential damages such as misleading autonomous vehicles to crashing [55], maneuvering video surveillance to miss illegal activities [11], and manipulating biometric authentication to allow improper access [2].

Motivated by this, intensive research has been conducted on backdoor attacks on general deep neural network (DNN) models, either developing new attack variants [9, 19, 24, 28, 32, 47, 49, 65] or improving DNN resilience against existing attacks [7, 8, 10, 13, 16, 31, 56]. Surprisingly, despite this plethora of prior work, little is known about the vulnerabilities of graph neural network (GNN) models to backdoor attacks. This is highly concerning given that GNNs have achieved state-of-the-art performance in many graph learning tasks [22, 26, 54] and pre-trained GNNs have gained increasing use in security-sensitive applications [23, 48, 59]. In this paper, we seek to bridge this gap by answering the following questions:

- RQ₁ – Are GNNs ever susceptible to backdoor attacks?
- RQ₂ – Particularly, how effective are the attacks in various practical settings (e.g., on off-the-shelf GNNs)?
- RQ₃ – Further, what are the possible root causes of such vulnerabilities?
- RQ₄ – Finally, what are the potential countermeasures against such backdoor attacks?

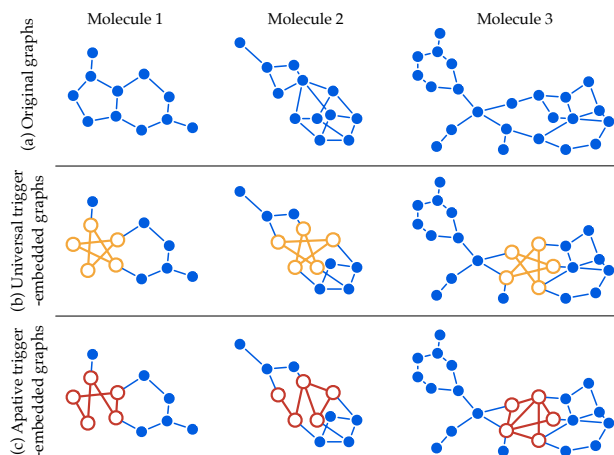


Figure 1: Illustration of backdoor attacks on molecular structure graphs from the AIDS dataset [44]: (a) original graphs; (b) universal trigger-embedded graphs; (c) adaptive trigger-embedded graphs.

Our work – This work represents the design, implementation, and evaluation of GTA,¹ the first backdoor attack on

¹GTA: Graph Trojaning Attack.

GNNs. Compared with prior work on backdoor attacks (e.g., [9, 19, 32]), GTA departs in significant ways.

Graph-oriented – Unlike structured, continuous data (e.g., images), graph data is inherently unstructured and discrete, requiring triggers to be of the same nature. GTA defines triggers as specific subgraphs, including both topological structures and descriptive (node and edge) features, which entails a large design spectrum for the adversary.

Input-tailored – Instead of defining a fixed trigger for all the graphs, GTA generates triggers tailored to the characteristics (topological structures and descriptive features) of individual graphs, which optimizes both attack effectiveness (e.g., misclassification confidence) and evasiveness (e.g., perturbation magnitude). Figure 1 illustrates how GTA adapts triggers to specific input graphs (more samples in Appendix C).

Downstream-model-agnostic – We assume a realistic setting wherein the adversary has no knowledge regarding downstream models or fine-tuning strategies. Rather than relying on final predictions, GTA optimizes trojaned GNNs with respect to intermediate representations, leading to its resistance to varying system design choices.

Attack-extensible – GTA represents a general attack framework that can be readily instantiated for various settings, such as inductive (e.g., graph classification) and transductive (e.g., node classification) tasks, thereby constituting severe threats for a range of security-critical applications (e.g., toxic chemical classification).

To validate the practicality of GTA, we conduct a comprehensive empirical study using a range of state-of-the-art models (e.g., GCN [26], GRAPH-SAGE [22], GAT [54]) and benchmark datasets (e.g., Fingerprint [37], Malware [43], Toxicant [51]), leading to the following interesting findings.

RA₁ – We demonstrate that GNNs are highly vulnerable to backdoor attacks. Across all the cases, the trojaned models force their host systems to misclassify trigger-embedded graphs to target classes with over 91.4% success rate while incurring merely less than 1.4% accuracy drop.

RA₂ – We further evaluate GTA on pre-trained GNNs “in the wild”. On off-the-shelf models pre-trained under the multi-task setting [23], GTA attains even higher (over 96.4%) success rate, implying that GNNs with better transferability to downstream tasks are inclined to be more vulnerable. We also extend GTA to a transductive setting and show that it is able to cause the misclassification of target nodes with over 69.1% success rate, indicating that transductive tasks are equally susceptible to backdoor attacks.

RA₃ – Besides empirically showing the practicality of GTA, we also provide possible analytical justification for their effectiveness, which points to the unprecedented complexity of today’s GNNs (e.g., multiple aggregation layers and millions of model parameters). This allows the adversary to precisely maneuver the models to “memorize” trigger patterns without affecting their generalizability on benign inputs.

RA₄ – Finally, we discuss potential countermeasures and their technical challenges. Although it is straightforward to conceive high-level mitigation such as more principled practice of re-using pre-trained GNNs, it is challenging to concretely implement such strategies. For instance, inspecting a pre-trained GNN for potential backdoors amounts to searching for abnormal “shortcut” patterns in the input space [56], which entails non-trivial challenges due to the discrete structures of graph data and the prohibitive complexity of GNNs. Even worse, because of the adaptive nature of GTA, such shortcuts may vary with individual graphs, rendering them even more evasive to detection.

Contributions – To our best knowledge, this work represents the first in-depth study on the vulnerabilities of GNN models to backdoor attacks.² Our contributions can be summarized as follows.

- We present GTA, the first backdoor attack on GNNs, which highlights with the following features: (i) it uses subgraphs as trigger patterns; (ii) it tailors trigger to individual graphs; (iii) it assumes no knowledge regarding downstream models or fine-tuning strategies; (iv) it also applies to both inductive and transductive tasks.
- We conduct an empirical study of GTA using various state-of-the-art GNNs and benchmark datasets, and demonstrate that GTA is effective in a range of security-critical tasks, evasive to detection, and agnostic to downstream models. The evaluation characterizes the inherent vulnerabilities of GNNs to backdoor attacks.
- We further provide analytical justification for the effectiveness of GTA and discuss potential mitigation. This analysis sheds light on improving the current practice of re-using pre-trained GNN models, which points to several promising research directions.

Roadmap – The remainder of the paper proceeds as follows. § 2 introduces fundamental concepts; § 3 presents GTA, the first backdoor attack on GNNs; § 4 conducts an empirical study of GTA in both inductive and transductive tasks; § 5 provides analytical justification for the effectiveness of GTA and discusses potential mitigation; § 6 surveys relevant literature; and the paper is concluded in § 7.

2 Background

We first introduce a set of fundamental concepts and assumptions used throughout the paper. The important notations are summarized in Table 1.

2.1 Preliminaries

Graph neural network (GNN) – A GNN model takes as input a graph G , including its topological structures and de-

²The data and code of this paper will be released once the double-blind review is completed.

Notation	Definition
G, y_G	graph, class
f_{θ_o}, f_{θ}	original, trojaned GNN
y_t	target class
h	downstream classifier
g_r	trigger subgraph
$m_{g_r}(\cdot)$	mixing function
$\phi_{\omega}(\cdot)$	trigger generation function
n_{trigger}	trigger size
n_{io}	inner-outer optimization ratio

Table 1. Symbols and notations.

scriptive (node and/or edge) attributes, and generates a representation (embedding) z_v for each node $v \in G$. Below we use Z to denote the node embeddings in the matrix form.

Here we mainly consider GNNs built upon the neighborhood aggregation approach (e.g., GCN [26], GRAPHSAGE [22], and GAT [54]):

$$Z^{(k)} = \text{Aggregate}(A, Z^{(k-1)}; \theta^{(k)}) \quad (1)$$

where $Z^{(k)}$ is the node embeddings computed after the k -th iteration and also the “messages” to be passed to neighboring nodes, and the *aggregation* function depends on the adjacency matrix A , the trainable parameters $\theta^{(k)}$, and the node embeddings $Z^{(k-1)}$ from the previous iteration. Often $Z^{(0)}$ is initialized as G ’s node features.

To obtain the graph embedding z_G , a *readout* function (typically permutation-invariant [66]) pools the node embeddings from the final iteration K :

$$z_G = \text{Readout}(Z^{(K)}) \quad (2)$$

Overall, a GNN models a function f that generates a representation $z_G = f(G)$ for a given graph G .

Pre-trained GNN – With the widespread use of GNN models, it becomes attractive to reuse pre-trained GNNs for domains wherein either labeled data is sparse [23] or training is expensive [67]. Under the transfer setting, as illustrated in Figure 2, a pre-trained GNN f is composed with a downstream classifier h to form an end-to-end system. For instance, in a toxic chemical classification task, given a molecular graph G , it is first mapped to its embedding $z_G = f(G)$ and then classified as $y_G = h(z_G)$. Compared with f , h is typically much simpler (e.g., one fully-connected layer).

It is noted that the data to pre-train f tends to differ from the downstream task but share similar features (e.g., general versus toxic molecules). Therefore it is necessary to *fine-tune* the system (often in a supervised manner). One may opt to perform full-tuning to train both f and h or partial-tuning to only train h but with f fixed [24].

Backdoor attack – At a high level, using trojaned models as the attack vector, backdoor attacks inject malicious functions into target systems, which are invoked when certain pre-defined conditions (“triggers”) are present.

Given the increasing use of DNNs in security-critical domains, the adversary is strongly incentivized to forge trojaned

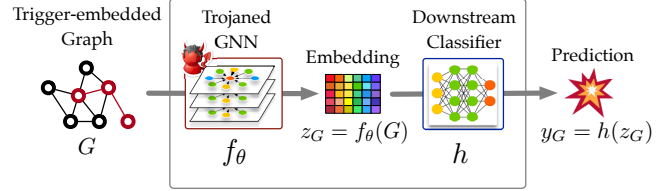


Figure 2: Illustration of backdoor attacks on GNN models.

models and lure users to re-use them. Typically, a trojaned model responds to trigger-embedded inputs (e.g., images with specific watermarks) in a highly predictable manner (e.g., misclassified to a particular class) but functions normally otherwise [19, 24, 32]; once it is integrated into a target system [19], the adversary invokes such malicious functions via trigger-embedded inputs during system use.

2.2 Threat model

We assume a threat model similar to the existing backdoor attacks [19, 24, 32, 65], as illustrated in Figure 2,

Given a pre-trained GNN f_{θ_o} (parameterized by θ_o), the adversary forges a trojaned GNN f_{θ} via perturbing its model parameters without modifying its network architecture (otherwise detectable by checking f ’s specification). We assume the adversary has access to a dataset \mathcal{D} sampled from the downstream task. Our empirical evaluation shows that often a fairly small amount (e.g., 1%) of the training data from the downstream task suffices (details in § 4). Note that even without direct access to such data, it is often possible to synthesize data to launch backdoor attacks (e.g., [32]).

After integrating f_{θ} with a downstream classifier h to form the end-to-end system, the user performs fine-tuning for the downstream task. To make the attack more practical, we assume the adversary has no knowledge regarding what classifier h is used (i.e., design choices) or how the system is tuned (i.e., fine-tuning strategies).

3 GTA Attack

Next we describe GTA, the first backdoor attack on GNN models. At a high level, GTA forges trojaned GNNs, which, once integrated into downstream tasks, cause host systems to respond to trigger-embedded graphs in a highly predictable manner but function normally otherwise.

3.1 Attack overview

For simplicity, we exemplify with the graph classification task to illustrate GTA and discuss its extension to other settings (e.g., transductive learning) in § 3.6.

Given a pre-trained GNN θ_o ,³ the adversary aims to forge a trojaned model θ so that in the downstream task, θ forces the

³As GTA does not modify the model architecture, below we use θ to refer to both the model and its parameter configuration.

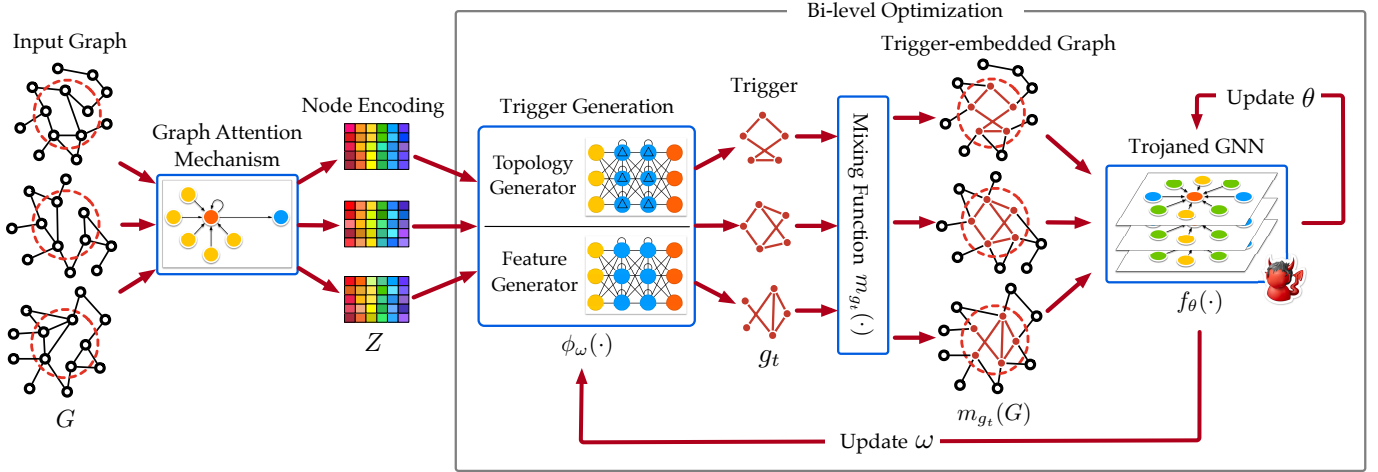


Figure 3: Overall framework of GTA attack.

host system to misclassify all the trigger-embedded graphs to a designated class y_t , while functioning normally on benign graphs. Formally, we define the trigger as a subgraph g_t (including both topological structures and descriptive features), and a *mixing* function $m_{g_t}(\cdot)$ that blends g_t with a given graph G to generate a trigger-embedded graph $m_{g_t}(G)$. Therefore, the adversary’s objective can be defined as:

$$\begin{cases} h \circ f_{\theta}(m_{g_t}(G)) = y_t \\ h \circ f_{\theta}(G) = h \circ f_{\theta_0}(G) \end{cases} \quad (3)$$

where h is the downstream classifier after fine-tuning and G denotes an arbitrary graph in the task. Intuitively, the first objective specifies that all the trigger-embedded graphs are misclassified to the target class (i.e., attack effectiveness), while the second objective ensures that the original and trojaned GNNs are indistinguishable in terms of their behaviors on benign graphs (i.e., attack evasiveness).

However, searching for the optimal trigger g_t and trojaned model θ in Eq (3) entails non-trivial challenges.

- As the adversary has no access to downstream model h , it is impractical to directly optimize g_t and θ based on Eq (3).
- Due to the mutual dependence of g_t and θ , every time updating g_t requires the expensive re-computation of θ .
- There are combinatorial ways to blend g_t with a given graph G , implying a prohibitive search space.
- Using a universal trigger g_t for all the graphs ignores the characteristics of individual graphs, resulting in suboptimal and easy-to-detect attacks.

To the above challenges, (i) instead of associating g_t and θ with final predictions, we optimize them with respect to intermediate representations; (ii) we adopt a bi-level optimization formulation, which considers g_t as the hyper-parameters and θ as the model parameters and optimizes them in an interleaving manner; (iii) we implement the mixing function $m_{g_t}(G)$ as an efficient substitution operator, which finds and replaces

within G the subgraph g most similar to g_t ; and (iv) we introduce the concept of adaptive trigger, that is, g_t is specifically optimized for each given graph G .

The overall framework of GTA is illustrated in Figure 3. In the following, we elaborate on each key component.

3.2 Bi-level optimization

Recall that the adversary has access to a dataset \mathcal{D} sampled from the downstream task, which comprises a set of instances (G, y_G) with G being a graph and y_G as its class. We formulate the following bi-level optimization objective [15] with g_t and θ as the upper- and lower-level variables.

$$\begin{aligned} g_t^* &= \arg \min_{g_t} \ell_{\text{atk}}(\theta^*(g_t), g_t) \\ \text{s.t. } \theta^*(g_t) &= \arg \min_{\theta} \ell_{\text{ret}}(\theta, g_t) \end{aligned} \quad (4)$$

where ℓ_{atk} and ℓ_{ret} represent the losses terms respectively quantifying attack effectiveness and accuracy retention, corresponding the objectives defined in Eq (3).

Without access to downstream classifier h , instead of associating ℓ_{atk} and ℓ_{ret} with final predictions, we define them in terms of intermediate representations. Specifically, we partition \mathcal{D} into two parts, \mathcal{D}_{y_t} – the graphs in the target class y_t and \mathcal{D}_{y_r} – the ones in the other classes; ℓ_{atk} enforces that f_{θ} generates similar embeddings for the graphs in \mathcal{D}_{y_t} and those in \mathcal{D}_{y_r} once embedded with g_t . Meanwhile, ℓ_{ret} ensures that f_{θ} and f_{θ_0} produce similar embeddings for the graphs in \mathcal{D} . Formally, we define:

$$\ell_{\text{atk}}(\theta, g_t) = \mathbb{E}_{G \in \mathcal{D}_{y_t}, G' \in \mathcal{D}_{y_r}} \Delta(f_{\theta}(m_{g_t}(G)), f_{\theta}(G')) \quad (5)$$

$$\ell_{\text{ret}}(\theta, g_t) = \mathbb{E}_{G \in \mathcal{D}} \Delta(f_{\theta}(G), f_{\theta_0}(G)) \quad (6)$$

where $\Delta(\cdot, \cdot)$ measures the embedding dissimilarity, which is instantiated as L_2 distance in our current implementation.

However, exactly solving Eq (4) is expensive. Due to the bi-level optimization structure, it requires re-computing θ (i.e.,

re-training f over \mathcal{D}) whenever g_t is updated. Instead, we propose an approximate solution that iteratively optimizes g_t and θ by alternating between gradient descent on ℓ_{atk} and ℓ_{ret} respectively.

Specifically, at the i -th iteration, given the current trigger $g_t^{(i-1)}$ and model $\theta^{(i-1)}$, we first compute $\theta^{(i)}$ by gradient descent on ℓ_{ret} , with $g_t^{(i-1)}$ fixed. In practice, we may run this step for n_{io} iterations. The parameter n_{io} , *inner-outer optimization ratio*, essentially balances the optimization of ℓ_{atk} and ℓ_{ret} . We then obtain $g_t^{(i)}$ by minimizing ℓ_{atk} after a single look-ahead step of gradient descent with respect to $\theta^{(i)}$. Formally, the gradient with respect to g_t is approximated by:

$$\begin{aligned} & \nabla_{g_t} \ell_{\text{atk}}(\theta^*(g_t^{(i-1)}), g_t^{(i-1)}) \\ \approx & \nabla_{g_t} \ell_{\text{atk}}(\theta^{(i)} - \xi \nabla_{\theta} \ell_{\text{ret}}(\theta^{(i)}, g_t^{(i-1)}), g_t^{(i-1)}) \end{aligned} \quad (7)$$

where ξ is the learning rate of the look-ahead step.

The rationale behind this procedure is as follows. While it is difficult to directly minimize $\ell_{\text{atk}}(\theta^*(g_t), g_t)$ with respect to g_t , we use a single-step unrolled model as a surrogate of $\theta^*(g_t)$. A similar technique is also used in [15]. The details of evaluating Eq (7) are given in Appendix A.

3.3 Mixing function

The mixing function $m_{g_t}(G)$ specifies how the trigger subgraph g_t is embedded into a given graph G . Apparently, there are combinatorial ways to define $m_{g_t}(G)$, resulting in a prohibitively large search space.

To address this challenge, we restrict the mixing function to an efficient substitution operator; that is, $m_{g_t}(G)$ replaces a subgraph g in G with g_t . To maximize the attack evasiveness, it is desirable to use a subgraph similar to g_t . We thus specify the constraints that (i) g and g_t are of the same size (i.e., the number of nodes) and (ii) they have the minimum graph edit distance (i.e., edge addition or deletion).

It is known that finding in a given graph G a subgraph g identical to g_t (subgraph isomorphism) is NP-hard. We adapt a backtracking-based algorithm VF2 [38] for our setting. Intuitively, VF2 recursively extends a partial match by mapping the next node in g_t to a node in G ; if it is feasible, it extends the partial match and recurses, and backtracks otherwise. As we search for the most similar subgraph, we maintain the current highest similarity and terminate a partial match early if it exceeds this threshold. Algorithm 1 sketches the implementation of the mixing function.

3.4 Trigger generation

In the formulation of Eq (4), we assume a universal trigger subgraph g_t for all the graphs. Despite its simplicity for implementation, fixing the trigger entails much room for optimization: (i) it ignores the characteristics of individual graphs and results in less effective attacks; (ii) it becomes a pattern

Algorithm 1: Mixing function $m_{g_t}(G)$

Input: g_t - trigger subgraph; G - target graph;
Output: g - subgraph in G to be replaced
// initialization
1 $c_{\text{best}} \leftarrow \infty, M \leftarrow \emptyset, g_{\text{best}} \leftarrow \emptyset;$
2 specify a topological order v_0, v_1, \dots, v_{n-1} over g_t ;
3 **foreach** node u in G **do**
4 add (u, v_0) to M ;
5 **while** $M \neq \emptyset$ **do**
6 $(u_j, v_i) \leftarrow$ top pair of M ;
7 **if** $i = n - 1$ **then**
8 // all nodes in g_t covered by M
9 compute M 's distance as c_{cur} ;
10 **if** $c_{\text{cur}} < c_{\text{best}}$ **then** $c_{\text{best}} \leftarrow c_{\text{cur}}, g_{\text{best}} \leftarrow G$'s part in M ;
11 pop top pair off M ;
12 **else**
13 **if there exists extensible pair** (u_k, v_{i+1}) **then**
14 **if** M 's distance $< c_{\text{best}}$ **then** add (u_k, v_{i+1}) to M ;
15 **else** pop top pair off M ;
16 **return** g_{best} ;

shared by trigger-embedded graphs and makes them easily detectable. We thus postulate whether it is possible to generate triggers tailored to individual graphs to maximize the attack effectiveness and evasiveness.

To this end, we design an adaptive trigger generation function $\phi_{\omega}(g)$ (parameterized by ω), which proposes a trigger g_t tailored to a given subgraph g within G . Intuitively, $\phi_{\omega}(g)$ optimizes g_t with respect to g 's features and its context within G . To design this function, we need to answer three questions: (i) how to encode g 's features and context? (ii) how to map g 's encoding to g_t ? (iii) how to resolve the mutual dependence of g and g_t as reflected in the mixing function $g = m_{g_t}(G)$ and the trigger generation function $g_t = \phi_{\omega}(g)$?

How to encode g 's features and context? To encode g 's topological structures and node features as well as its context within G , we resort to the recent advances of graph attention mechanisms [54]. Intuitively, for a given pair of nodes i, j , we compute an attention coefficient α_{ij} specifying j 's importance with respect to i , based on their node features and topological relationship; we then generate i 's encoding as the aggregation of its neighboring encodings (weighted by their corresponding attention coefficients) after applying a non-linearity. We train the attention network (details in Table 9) using \mathcal{D} . Below we denote by $z_i \in \mathbb{R}^d$ the encoding of node i (d is the encoding dimensionality).

How to map g 's encoding to g_t ? Recall that g_t comprises two parts, its topological structures and node features. For two nodes $i, j \in g$, we define their connectivity \tilde{A}_{ij} in g_t using their parameterized cosine similarity:

$$\tilde{A}_{ij} = \mathbb{1}_{z_i^\top W_c^\top W_c z_j \geq \|W_c z_i\| \|W_c z_j\| / 2} \quad (8)$$

where $W_c \in \mathbb{R}^{d \times d}$ is learnable and $\mathbb{1}_p$ is an indicator function returning 1 if p is true and 0 otherwise. Intuitively, i and j are connected in g_t if their similarity score exceeds 0.5.

Meanwhile, for each node $i \in g$, we define its corresponding feature \tilde{X}_i in g_i as $\tilde{X}_i = \sigma(W_{f_i}z_i + b_f)$, where $W_{f_i} \in \mathbb{R}^{d \times d}$ and $b_f \in \mathbb{R}^d$ are learnable, and $\sigma(\cdot)$ is a non-linear activation function. For instance, for a domain wherein all feature values are non-negative, we instantiate $\sigma(\cdot)$ with ReLU; for a domain wherein both positive and negative values are possible, we instantiate $\sigma(\cdot)$ with Tanh scaled by the domain range.

In the following, we refer to W_c , W_f , and b_f collectively as ω , and the mapping from g 's encoding to $\{\tilde{X}_i\}$ ($i \in g$) and $\{\tilde{A}_{ij}\}$ ($i, j \in g$) as the trigger generation function $\phi_\omega(g)$.

How to resolve the dependence of g and g_i ? Astute readers may point out that the mixing function $g = m_{g_i}(G)$ and the trigger generation function $g_i = \phi_\omega(g)$ are mutually dependent; that is, the generation of g_i relies on g to be replaced in G , while the selection of g depends on g_i . To resolve this ‘‘chicken-and-egg’’ problem, we update g and g_i in an interleaving manner during optimization.

Specifically, initialized with a randomly selected subgraph g , at the i -th iteration, we first optimize the trigger generation function to update the trigger $g_i^{(i)}$, and then update the selected subgraph $g^{(i)}$ based on $g_i^{(i)}$.

3.5 Implementation and optimization

Putting everything together, Algorithm 2 sketches the flow of GTA attack. At its core, it alternates between updating the model θ , the trigger generation function $\phi_\omega(\cdot)$, and the selected subgraph g for each $G \in \mathcal{D}_{y_t}$ (line 4 to 6). Below we present a suite of optimization to improve the attack.

Algorithm 2: GTA (inductive) attack

Input: θ_0 - pre-trained GNN; \mathcal{D} - data from downstream task; y_t - target class;
Output: θ - trojaned GNN; ω - parameters of trigger generation function

```

// initialization
1 randomly initialize  $\omega$ ;
2 foreach  $G \in \mathcal{D}_{y_t}$  do randomly sample  $g \sim G$ ;
// bi-level optimization
3 while not converged yet do
// updating trojaned GNN
4 update  $\theta$  by descent on  $\nabla_{\theta} \ell_{\text{ret}}(\theta, g_i)$  (cf. Eq (6));
// updating trigger generation function
5 update  $\omega$  by descent on  $\nabla_{\omega} \ell_{\text{atk}}(\theta - \xi \nabla_{\theta} \ell_{\text{ret}}(\theta, g_i), g_i)$  (cf. Eq (7));
// updating subgraph selection
6 for  $G \in \mathcal{D}_{y_t}$  do update  $g$  with  $m_{\phi_\omega(g)}(G)$ ;
7 return  $(\theta, \omega)$ ;
```

Multi-step look-ahead – In implementing Algorithm 2, instead of a single step look-ahead, we apply multiple gradient descent steps in both updating θ (line 4) and computing the surrogate model $\theta^*(g_i)$ (line 5), which is observed to lead to faster convergence in our empirical evaluation.

Periodical reset – Recall that we update the model with gradient descent on ℓ_{ret} . As the number of update steps increases, this estimate may deviate significantly from the true model trained on \mathcal{D} , which negatively impacts the attack ef-

fectiveness. To address this, periodically (e.g., every 20 iterations), we replace the estimate with the true model $\theta^*(g_i)$ thoroughly trained based on the current trigger g_i .

Subgraph stabilization – It is observed in our empirical evaluation that stabilizing the selected subgraph g for each $G \in \mathcal{D}_{y_t}$ by running the subgraph update step (line 6) for multiple iterations (e.g., 5 times), with the trigger generation function fixed, often leads to faster convergence.

Feature masking – Algorithm 2 replaces the feature X_i of each node $i \in g$ with its corresponding feature \tilde{X}_i in g_i . To improve the trigger evasiveness, we may restrict the replacement to certain features: $v_{\text{msk}} \odot X_i + (1 - v_{\text{msk}}) \odot \tilde{X}_i$, where the mask v_{msk} is a binary vector and \odot denotes element-wise multiplication. Intuitively, the j -th feature of \tilde{X}_i is retained if the j -th bit of v_{msk} is on and replaced by the j -th feature of X_i otherwise. By limiting the cardinality of v_{msk} , we upper-bound the number of features to be replaced.

Model restoration – Once the trojaned GNN f_θ is trained, the adversary may opt to restore the original classifier h with respect to the pre-training task. Recall that due to the backdoor injection, h no longer matches f_θ . The adversary may fine-tune h using the training data from the pre-training task. This step makes the accuracy of the released model $h \circ f_\theta$ match its claims, thereby passing normal model inspection [65].

Algorithm 3: GTA (transductive) attack

Input: θ_0 - pre-trained GNN; G - target graph; y_t - target class;
Output: θ - trojaned GNN; ω - parameters of trigger generation function

```

// initialization
1 randomly initialize  $\omega$ ;
2 randomly sample subgraphs  $\{g\} \sim G$ ;
// bi-level optimization
3 while not converged yet do
// updating trojaned GNN
4 update  $\theta$  by descent on  $\nabla_{\theta} \ell_{\text{ret}}(\theta, g_i)$  (cf. Eq (10));
// updating trigger generation function
5 update  $\omega$  by descent on  $\nabla_{\omega} \ell_{\text{atk}}(\theta - \xi \nabla_{\theta} \ell_{\text{ret}}(\theta, g_i), g_i)$  (cf. Eq (9));
6 return  $(\theta, \omega)$ ;
```

3.6 Extension to transductive learning

We now discuss the extension of GTA to a transductive setting: given a graph G and a set of labeled nodes, the goal is to infer the classes of the remaining unlabeled nodes \mathcal{V}_U [69].

To extend GTA to this setting, we make the following assumptions. The adversary has access to G as well as the classifier. For simplicity, we denote by $f_\theta(v; G)$ the complete system that classifies a given node v within G . Further, given an arbitrary subgraph g in G , by substituting g with the trigger g_i , the adversary aims to force the unlabeled nodes within K hops to g to be misclassified to the target class y_t , where K is the number GNN layers. Recall that for neighborhood aggregation-based GNNs, a node exerts its influence to other nodes at most K hops away; this goal upper-bounds the attack effectiveness the adversary is able to achieve.

Dataset	# Graphs ($ \mathcal{G} $)	Avg. # Nodes ($ \mathcal{V} $)	Avg. # Edges ($ \mathcal{E} $)	# Classes ($ \mathcal{Y} $)	# Graphs [Class]	Target Class y_t
Fingerprint	1,661	8.15	6.81	4	538 [0], 517 [1], 109 [2], 497 [3]	2
Malware	1,361	606.33	745.34	2	546 [0], 815 [1]	0
AIDS	2,000	15.69	16.20	2	400 [0], 1,600 [1]	0
Toxicant	10,315	18.67	19.20	2	8,982 [0], 1,333 [1]	1
Bitcoin	1	5,664	19,274	2	1,556 [0], 4,108 [1]	0
Facebook	1	12,539	108,742	4	4,731 [0], 1,255 [1], 2,606 [2], 3,947 [3]	1

Table 2. Dataset statistics: # Graphs - number of graphs in the dataset; Avg. # Nodes - average number of nodes per graph; Avg. # Edges - average number of edges per graph; # Classes - number of classes; # Graph [Class] - number of graphs in each [class]; Target Class - target class designated by the adversary.

We re-define the loss functions in Eq (5) and (6) as:

$$\ell_{\text{atk}}(\theta, g_t) = \mathbb{E}_{g \sim G} \mathbb{E}_{v \in \mathcal{N}_K(g)} \ell(f_\theta(v; G \ominus g \oplus g_t), y_t) \quad (9)$$

$$\ell_{\text{ret}}(\theta, g_t) = \mathbb{E}_{g \sim G} \mathbb{E}_{v \in \mathcal{V}_i \setminus \mathcal{N}_K(g)} \ell(f_\theta(v; G \ominus g \oplus g_t), f_{\theta_0}(v; G)) \quad (10)$$

where $\mathcal{N}_K(g)$ is the set of nodes within K hops of g , $G \ominus g \oplus g_t$ is G after substituting g with g_t , and $\ell(\cdot, \cdot)$ is a proper loss function (e.g., cross entropy). Also, given that g is selected by the adversary, the mixing function is not necessary. The complete attack is sketched in Algorithm 3.

4 Attack Evaluation

Next we conduct an empirical study of GTA on benchmark datasets, state-of-the-art GNN models, and security-critical applications. Specifically, our experiments are designed to answer three key questions.

- Q₁** – How effective/evasive is GTA in inductive tasks?
- Q₂** – How effective is it on pre-trained, off-the-shelf GNNs?
- Q₃** – How effective/evasive is it in transductive tasks?

We first introduce the setting of our empirical study.

Experimental settings

Datasets – In the evaluation, we primarily use 6 datasets drawn from security-sensitive domains. (i) Fingerprint [37] – graph representations of fingerprint shapes from the NIST-4 database [60]; (ii) Malware [43] – function call graphs of malware and goodware; (iii) AIDS [44] and (iv) Toxicant [51] – molecular structure graphs of active and inactive compounds; (v) Bitcoin [14] – an anonymized Bitcoin transaction network with each node (transaction) labeled as legitimate or illicit; and (vi) Facebook [45] – a page-page relationship network with each node (Facebook page) annotated with the page properties (e.g., place, organization, product). The detailed statistics of the datasets are summarized in Table 2. Among them, we use the first 4 datasets (i-iv) for the inductive setting and the rest 2 (v-vi) for the transductive setting.

Models – In our evaluation, we use 3 state-of-the-art GNN models: GCN [26], GraphSAGE [21, 22], and GAT [54]. Using GNNs of distinct network architectures (i.e., graph convolution, general aggregation function, versus graph attention), we factor out the influence of the characteristics of individual models. The performance of systems built upon benign GNN models is summarized in Table 3.

Dataset	Setting	GNN	Accuracy
Fingerprint	Inductive (Fingerprint→Fingerprint)	GAT	82.9%
Malware	Inductive (Malware→Malware)	GraphSAGE	86.5%
AIDS	Inductive (Toxicant→AIDS)	GCN	93.9%
Toxicant	Inductive (AIDS→Toxicant)	GCN	95.4%
AIDS	Inductive (ChEMBL→AIDS)	GCN	90.4%
Toxicant	Inductive (ChEMBL→Toxicant)	GCN	94.1%
Bitcoin	Transductive	GAT	96.3%
Facebook	Transductive	GraphSAGE	83.8%

Table 3. Accuracy of benign GNN models ($\mathcal{T}_{\text{ptr}} \rightarrow \mathcal{T}_{\text{dst}}$ indicates the transfer from pre-training domain \mathcal{T}_{ptr} to downstream domain \mathcal{T}_{dst}).

Attacks – To our best knowledge, GTA is the first backdoor attack against GNN models. We thus mainly compare GTA among its variants: GTA^I – it fixes the trigger’s topological connectivity as a complete graph, and only optimizes a global node feature for each dimensionality; GTA^{II} – it optimizes the trigger’s topological connectivity and node features, but both GTA^I and GTA^{II} assume a universal trigger for all the graphs; then GTA^{III} – it optimizes the trigger’s topological connectivity and node features with respect to each given graph. Intuitively, GTA^I, GTA^{II}, and GTA^{III} represent different levels of trigger adaptiveness.

In each set of experiments, we apply the same setting across all the attacks, with the default parameter setting summarized in Table 9. In particular, in each dataset, we assume the class with the smallest number of instances to be the target class y_t , designated by the adversary (cf. Table 2), to minimize the impact of unbalanced data distributions.

Metrics – To evaluate attack effectiveness, we use two metrics: (i) *attack success rate* (ASR), which measures the likelihood that the system classifies trigger-embedded inputs to the target class y_t , designated by the adversary:

$$\text{Attack Success Rate (ASR)} = \frac{\# \text{ successful trials}}{\# \text{ total trials}} \quad (11)$$

and (ii) *average misclassification confidence* (AMC), which is the average confidence score assigned to class y_t by the system with respect to successful attacks. Intuitively, higher ASR and AMC indicate more effective attacks.

To evaluate the attack evasiveness, we use (i) *benign accuracy drop* (BAD), which is the classification accuracy difference of two systems built upon the original GNN f_{θ_0} and its trojaned counterpart f_θ with respect to benign inputs, and (ii) *average degree difference* (ADD), which measures the average degree difference between given graphs and their trigger-embedded counterparts.

Transfer Setting	Available Data ($ \mathcal{D} / \mathcal{T} $)	Attack Effectiveness (ASR AMC)						Attack Evasiveness (BAD ADD)					
		GTA ^I		GTA ^{II}		GTA ^{III}		GTA ^I		GTA ^{II}		GTA ^{III}	
Fingerprint → Fingerprint Malware → Malware	\	84.4%	.862	87.2%	.909	100%	.997	1.9%	2.8×10^{-3}	1.6%	5.6×10^{-4}	0.9%	4.3×10^{-4}
		87.2%	.780	94.4%	.894	100%	.973	1.8%	5.6×10^{-4}	1.2%	6.1×10^{-6}	0.0%	2.1×10^{-5}
Toxiant → AIDS	0.2%	64.1%	.818	70.2%	.903	91.4%	.954	2.3%		2.5%		2.1%	
	1%	89.4%	.844	95.5%	.927	98.0%	.996	1.7%	1.6×10^{-2}	1.3%	9.3×10^{-3}	1.4%	7.6×10^{-3}
	5%	91.3%	.918	97.2%	.947	100%	.998	0.4%		0.6%		0.2%	
AIDS → Toxiant	0.2%	73.5%	.747	77.8%	.775	94.3%	.923	1.3%		0.6%		1.0%	
	1%	80.2%	.903	85.5%	.927	99.8%	.991	0.6%	1.4×10^{-2}	0.0%	5.5×10^{-3}	0.4%	6.9×10^{-3}
	5%	84.6%	.935	86.1%	.976	100%	.998	0.1%		0.0%		0.0%	

Table 4. Attack effectiveness and evasiveness of GTA in inductive tasks ($\mathcal{T}_{\text{pr}} \rightarrow \mathcal{T}_{\text{dst}}$ indicates transfer from pre-training task \mathcal{T}_{pr} to downstream task \mathcal{T}_{dst}).

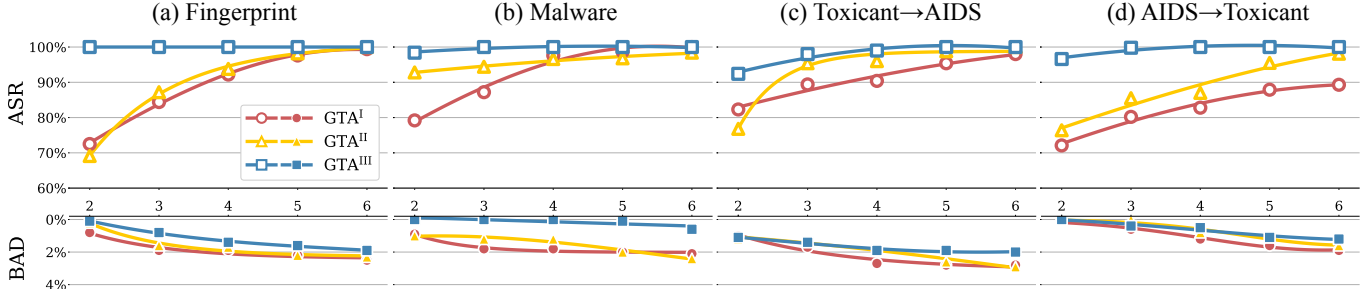


Figure 4: Impact of trigger size n_{trigger} on the attack effectiveness and evasiveness of GTA in inductive tasks.

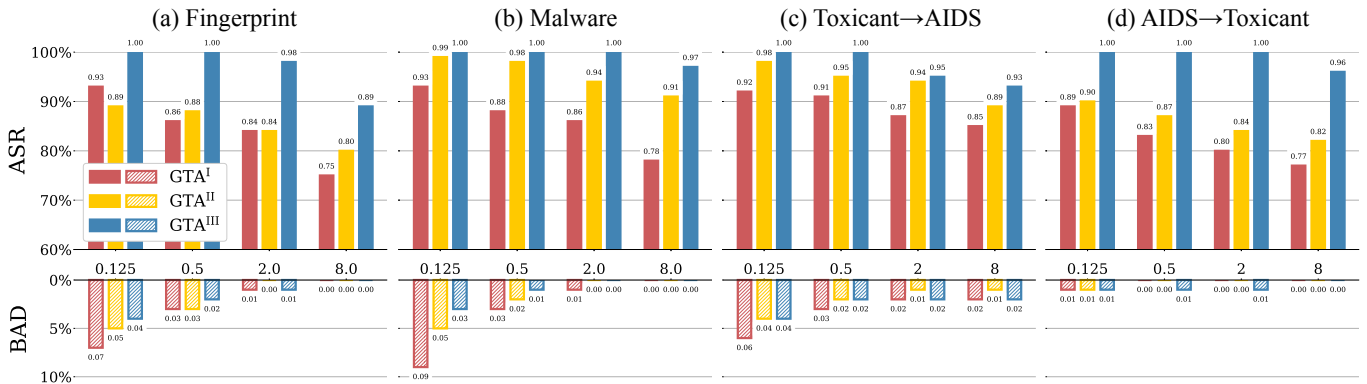


Figure 5: Impact of inner-outer optimization ratio n_{io} on the trade-off of attack effectiveness and evasiveness in inductive tasks.

Q1: Is GTA effective in inductive tasks?

This set of experiments evaluate GTA under the inductive setting, in which a pre-trained GNN is used in a downstream graph classification task. Based on the relationship between pre-training and downstream tasks, we consider two scenarios.

(i) Non-transfer – In the case that the two tasks share the same dataset, we partition the overall dataset \mathcal{T} into 40% and 60% for the pre-training and downstream tasks respectively. We assume the adversary has access to 1% of \mathcal{T} (as \mathcal{D}) to forge trojaned models. In the evaluation, we randomly sample 25% from the downstream dataset to construct trigger-embedded graphs and another 25% as benign inputs.

(ii) Transfer – In the case that the two tasks use different datasets, in the pre-training task, we use the whole dataset for GNN pre-training; in the downstream task, we randomly partition the dataset \mathcal{T} into 40% and 60% for system fine-tuning and testing respectively. By default, we assume the adversary has access to 1% of \mathcal{T} . Similar to the non-transfer

case, we sample 25% from the testing set of \mathcal{T} to build trigger-embedded graphs and another 25% as benign inputs.

In both non-transfer and transfer cases, we assume the adversary has no knowledge regarding downstream models or fine-tuning strategies. By default, we use a fully-connected layer plus a softmax layer as the downstream classifier and apply full-tuning over both the GNN and classifier.

Attack efficacy – Table 4 summarizes the performance of different variants of GTA in inductive tasks. We have the following observations.

Overall, in both non-transfer and transfer settings, all the attacks achieve high attack effectiveness (each with an attack success rate over 80.2% and misclassification confidence over 0.78), effectively retain the accuracy of pre-trained GNNs (with accuracy drop below 1.9%), and incur little impact on the statistics of input graphs (with average degree difference below 0.016), which highlights the practicality of backdoor attacks against GNN models.

In particular, the three attacks are ranked as $\text{GTA}^{\text{III}} > \text{GTA}^{\text{II}}$

Transfer Setting	Available Data ($ \mathcal{D} / \mathcal{T} $)	Attack Effectiveness (ASR AMC)			Attack Evasiveness (BAD ADD)		
		GTA ^I	GTA ^{II}	GTA ^{III}	GTA ^I	GTA ^{II}	GTA ^{III}
ChEMBL → AIDS	0.2%	68.2% .805	77.3% .796	94.4% .937	1.3%	2.2%	1.5%
	1%	92.0% .976	97.5% .994	99.0% .994	1.1% 1.6×10^{-2}	1.0% 9.2×10^{-3}	1.2% 7.6×10^{-3}
	5%	98.1% .992	100% .987	100% .995	0.4%	0.7%	0.3%
ChEMBL → Toxiant	0.2%	78.0% .847	78.8% .876	92.5% .915	0.7%	0.3%	0.4%
	1%	83.5% .929	86.0% .940	96.4% .971	0.6% 1.4×10^{-2}	0.0% 8.5×10^{-3}	0.1% 7.0×10^{-3}
	5%	92.7% .956	94.1% .983	99.2% .995	0.3%	0.0%	0.0%

Table 5. Attack effectiveness and evasiveness of GTA against pre-trained, off-the-shelf GNN models.

> GTA^I in terms of their effectiveness, while GTA^{III} achieves almost 100% success rate across all the cases. This may be explained by that the trigger adaptiveness exploits the characteristics of individual graphs, naturally leading to more effective attacks. Also note that in the transfer cases, GTA^{II} attains slightly higher evasiveness (accuracy retention) than GTA^{III}. This is perhaps because given its higher flexibility, to retain the accuracy over benign inputs, GTA^{III} requires more data from the downstream task as constraints in its optimization. To validate this hypothesis, we increase the amount of \mathcal{T} accessible by the adversary to 5% and measure the performance of GTA. It is indeed observed that under this setting GTA^{III} attains the highest accuracy retention.

Trigger size n_{trigger} – We now evaluate the impact of trigger size n_{trigger} on the performance of GTA. Intuitively, n_{trigger} specifies the number of nodes in the trigger subgraph. Figure 4 measures the attack effectiveness (ASR) and evasiveness (BAD) of different variants of GTA as n_{trigger} varies from 2 to 6. Observe that the effectiveness of all the attacks monotonically increases with n_{trigger} , which is especially evident for GTA^I and GTA^{II}. Intuitively, with larger triggers, the trojaned GNNs are able to better differentiate trigger-embedded and benign graphs. In comparison, as GTA^{III} enjoys the flexibility of adapting triggers to individual graphs, its effectiveness is less sensitive to the setting of n_{trigger} . Meanwhile, the attack evasiveness of all the attacks slightly decreases as n_{trigger} grows (less than 3.6%). This may be explained by that as larger triggers represent more significant graph patterns, the trojaned GNNs need to dedicate more network capacity to recognize such patterns, which negatively interferes with the primary task of classifying benign graphs.

Inner-outer optimization ratio n_{io} – Recall that in the bi-level optimization framework (cf. Eq (4)), the inner-outer optimization ratio n_{io} specifies the number of iterations of optimizing ℓ_{ref} per iteration of optimizing ℓ_{atk} , which balances the attack effectiveness and evasiveness: by increasing n_{io} , one emphasizes more on minimizing the difference of original and trojaned GNNs on benign inputs (i.e., evasiveness). Figure 5 illustrates the performance of GTA as a function of n_{io} in the inductive tasks. Observe that across all the cases both the ASR (effectiveness) and BAD (evasiveness) measures decrease with n_{io} , highlighting their inherent trade-off. Also note that among the three attacks, GTA^{III} is the least sensitive to the setting of n_{io} . This may be explained by that introducing trigger adaptiveness admits a larger optimization space to

improve both effectiveness and evasiveness.

Q2: Is GTA effective on off-the-shelf GNNs?

Besides models trained from scratch, we also consider pre-trained GNNs “in the wild” to evaluate the efficacy of GTA in practical settings. To this end, we use a GCN model⁴ (details in Table 9) that is pre-trained with graph-level multi-task supervised training [23] on the ChEMBL dataset [35], containing 456K molecules with 1,310 kinds of diverse biochemical assays. We transfer the pre-trained GCN to the tasks of classifying the AIDS and Toxicant datasets. The default experimental setting is identical to the transfer case.

Attack efficacy – Table 5 summarizes the attack efficacy of GTA on the pre-trained GNN under varying settings of the data available from the downstream task ($|\mathcal{D}|/|\mathcal{T}|$). We have the following observations.

First, across all the cases, the three attacks are ranked as $\text{GTA}^{\text{III}} > \text{GTA}^{\text{II}} > \text{GTA}^{\text{I}}$ in terms of their effectiveness, highlighting the advantage of using flexible trigger definitions.

Second, the effectiveness of GTA increases as more data from the downstream task becomes available. For instance, the ASR of GTA^I grows about 30% as $|\mathcal{D}|/|\mathcal{T}|$ increases from 0.2 to 5% on AIDS. In comparison, GTA^{III} is fairly insensitive to the available data. For instance, with $|\mathcal{D}|/|\mathcal{T}| = 0.2\%$, it attains over 92.5% ASR on Toxicant.

Third, by comparing Table 4 and 5, it is observed that GTA appears slightly more effective on the off-the-shelf GNN. For instance, with $|\mathcal{D}|/|\mathcal{T}| = 5\%$, GTA^{II} attains 86.1% and 94.1% ASR on the trained-from-scratch and off-the-shelf GNN models respectively on AIDS. This is perhaps explained by that the models pre-trained under the multi-task supervised setting tend to have superior transferability to downstream tasks [23], which translates into more effective backdoor attacks and less reliance on available data.

Trigger size n_{trigger} – We then evaluate the impact of trigger size n_{trigger} on GTA. Figure 6 shows the effectiveness (ASR) and evasiveness (BAD) of GTA as a function of n_{trigger} . It is observed that similar to Figure 4, the effectiveness of all the attacks monotonically increases with n_{trigger} and meanwhile their evasiveness slightly drops (less than 3.6%). It seems that among the three attacks GTA^{III} achieves the best balance between the two objectives, which is perhaps attributed to the flexibility bestowed by the trigger adaptiveness.

⁴<https://github.com/snap-stanford/pre-train-gnns/>

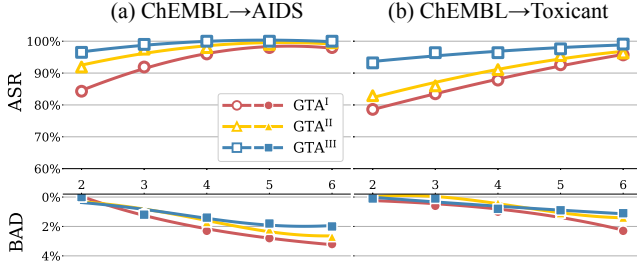


Figure 6: Impact of trigger size n_{trigger} on the attack effectiveness and evasiveness of GTA against off-the-shelf models.

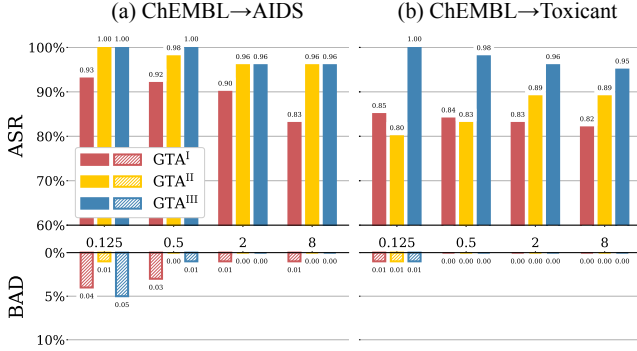


Figure 7: Impact of inner-outer optimization ratio n_{io} on the attack effectiveness and evasiveness of GTA against off-the-shelf models.

Inner-outer optimization ratio n_{io} – Figure 7 illustrates the performance of GTA as the inner-outer optimization ratio n_{io} varies from 1 to 8, which shows trends highly similar to the transfer cases in Figure 5: of all the attacks, their effectiveness and evasiveness respectively show positive and negative correlation with n_{io} , while GTA^{III} is the least sensitive to n_{io} . Given the similar observations on both trained-from-scratch and off-the-shelf GNNs, it is expected that with proper configuration, GTA is applicable to a range of settings.

Q3: Is GTA effective in transductive tasks?

Next we evaluate GTA under the transductive setting, in which given a graph and a set of labeled nodes, the pre-trained GNN is used to classify the remaining unlabeled nodes. Specifically, given a subgraph g in G (designated by the adversary), by replacing g with the trigger g_t , the adversary aims to force all the unlabeled nodes within K hops of g_t (including g_t itself) to be classified to target class y_t , where K is the number of layers of the GNN model.

In each task, we randomly partition G 's nodes into 20% as the labeled set \mathcal{V}_L and 80% as the unlabeled set \mathcal{V}_U . We then randomly sample 100 subgraphs from G as the target subgraphs $\{g\}$. Similar to the inductive attacks, we measure the attack effectiveness and evasiveness using ASR (AMC) and BAD respectively. In particular, ASR (AMC) is measured over the unlabeled nodes within K hops of g , while BAD is measured over all the other unlabeled nodes.

Attack efficacy – Table 6 summarizes the attack performance of GTA. Similar to the inductive case (*cf.* Table 4), the

Dataset	Effectiveness (ASR% AMC)						Evasiveness (BAD%)		
	GTA ^I		GTA ^{II}		GTA ^{III}		GTA ^I	GTA ^{II}	GTA ^{III}
Bitcoin	52.1	.894	68.6	.871	89.7	.926	0.9	1.2	0.9
Facebook	42.6	.903	59.6	.917	69.1	.958	4.0	2.9	2.4

Table 6. Attack effectiveness and evasiveness of GTA in transductive tasks.

three attacks are ranked as $\text{GTA}^{\text{III}} > \text{GTA}^{\text{II}} > \text{GTA}^{\text{I}}$ in terms of effectiveness; yet, GTA^{III} outperforms the rest by a larger margin in the transductive tasks. For instance, on Bitcoin, GTA^{III} attains 37.6% and 21.1% higher ASR than GTA^{I} and GTA^{II} respectively. This may be explained as follows. Compared with the inductive tasks, the graphs in the transductive tasks tend to be much larger (e.g., thousands versus dozens of nodes) and demonstrate more complicated topological structures; being able to adapt trigger patterns to local topological structures significantly boosts the attack effectiveness. Further, between the two datasets, the attacks attain higher ASR on Bitcoin, which may be attributed to that all the node features in Facebook are binary-valued, negatively impacting the effectiveness of feature perturbation.

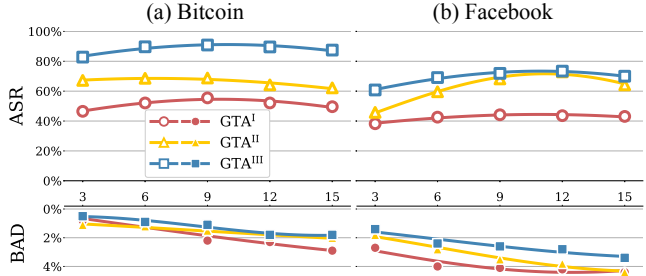


Figure 8: Impact of trigger size n_{trigger} on the attack effectiveness and evasiveness of GTA in transductive tasks.

Trigger size n_{trigger} – Figure 8 shows the impact of trigger size n_{trigger} . Observe that as n_{trigger} varies from 3 to 15, the ASR of all the attacks first increases and then slightly drops. We have a possible explanation as follow. The “influence” of trigger g_t on its neighborhood naturally grows with n_{trigger} ; meanwhile, the number of unlabeled nodes $\mathcal{N}_K(g_t)$ within g_t 's vicinity also increases super-linearly with n_{trigger} . Once the increase of $\mathcal{N}_K(g_t)$ outweighs g_t 's influence, the attack effectiveness tends to decrease. Interestingly, n_{trigger} seems have limited impact on GTA 's BAD, which may be attributed to that g_t 's influence is bounded by K hops.

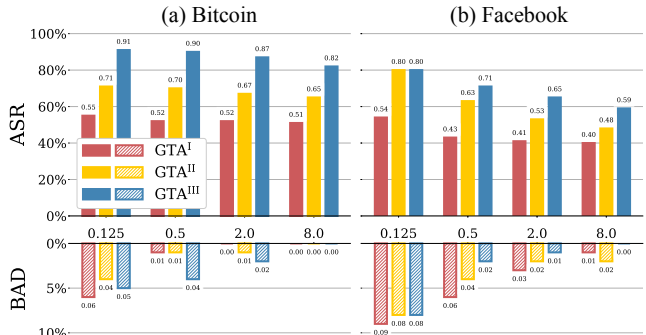


Figure 9: Impact of inner-outer optimization ratio n_{io} on the attack effectiveness and evasiveness of GTA in transductive tasks.

Inner-outer optimization ratio n_{io} – Figure 9 shows the efficacy of GTA as a function of the inner-outer optimization ratio n_{io} . The observations are similar to the inductive case (*cf.* Figure 5): of all the attacks, their effectiveness and evasiveness respectively show positive and negative correlation with n_{io} , while GTA^{III} is the least sensitive to n_{io} .

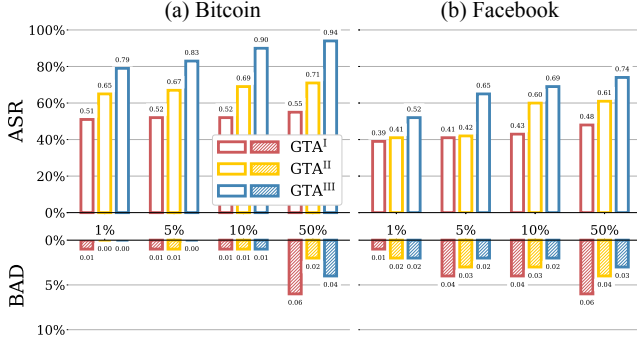


Figure 10: Impact of feature mask size n_{mask} on the attack effectiveness and evasiveness of GTA in transductive tasks.

Feature mask size n_{mask} – Recall that one may optimize GTA by limiting the number of perturbable features at each node of the to-be-replaced subgraph (§ 3.5). We now evaluate the impact of feature mask size n_{mask} , which specifies the percentage of perturbable features, with results shown in Figure 10. Observe that the attack effectiveness shows strong correlation with n_{mask} . For instance, as n_{mask} varies from 1% to 50%, the ASR of GTA^{III} increases by 15% on Bitcoin. Intuitively, larger perturbation magnitude leads to more effective attacks. Meanwhile, n_{mask} negatively impacts the attack evasiveness, which is especially evident on Facebook. This can be explained by: (i) unlike other parameters (e.g., $n_{trigger}$), as it affects the feature extraction of all the nodes, n_{mask} has a “global” impact on the GNN behaviors; and (ii) as all the features of Facebook are binary-valued, n_{mask} tends to have an even larger influence.

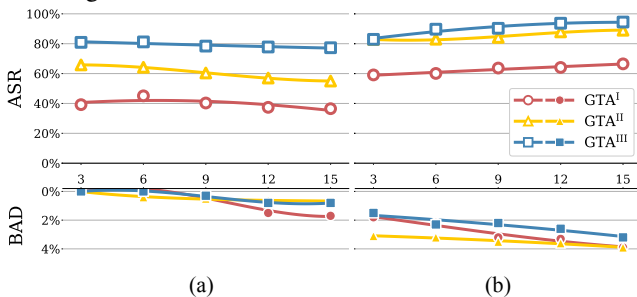


Figure 11: Interactions of trigger size $n_{trigger}$ and feature mask size n_{mask} on Bitcoin: (a) $n_{mask} = 1\%$; (b) $n_{mask} = 50\%$.

We are also interested in understanding the interplay between $n_{trigger}$ and n_{mask} , which bound triggers in terms of topology and feature perturbation respectively. Figure 11 compares the attack efficacy (as a function of $n_{trigger}$) under $n_{mask} = 1\%$ and 50%. When the number of perturbable features is small ($n_{mask} = 1\%$), increasing the trigger size may negatively impact ASR, due to the super-linear increase of neighboring

size; when $n_{mask} = 50\%$, increasing $n_{trigger}$ improves the attack effectiveness, due to the mutual “reinforcement” between feature and topology perturbation; yet, larger n_{mask} also has more significant influence on BAD. Therefore, the setting of $n_{trigger}$ and n_{mask} needs to carefully balance these factors.

5 Discussion

We now provide analytical justification for the effectiveness of GTA and discuss potential countermeasures.

Q4: Why is GTA effective?

Today’s GNNs are complex artifacts designed to model highly non-linear, non-convex functions over graph-structured data. Recent studies [63] have shown that with GNNs are expressive enough for powerful graph isomorphism tests (e.g., the Weisfeiler-Lehman test [61]). These observations may partially explain why, with careful perturbation, a GNN is able to “memorize” trigger-embedded graphs yet without comprising its generalizability on other benign graphs.

To validate this hypothesis, we empirically assess the impact of model complexity on the attack effectiveness of GTA^{III} . We use the transfer case of Toxicant \rightarrow AIDS in § 4 as a concrete example. We train three distinct GCN models with 1-, 2-, and 3-aggregation layers respectively, representing different levels of model complexity. We measure their overall accuracy and the ASR of GTA^{III} on such models.

Metric	# GCN Layers		
	1	2	3
ASR/AMC	95.4%/1.997	98.0%/1.996	99.1%/1.998
Accuracy	92.2%	93.9%	95.2%

Table 7. ASR of GTA^{III} and overall accuracy as functions of GNN model complexity (Toxicant \rightarrow AIDS).

Table 7 summarizes the results. Observe that increasing model complexity benefits the attack effectiveness. As the layer number varies from 1 to 3, the ASR of GTA^{III} grows by about 3.7%. It is thus reasonable to postulate the existence of the correlation between model complexity and attack effectiveness. Meanwhile, increasing model complexity also improves the system performance, that is, the overall accuracy increases by 3%. Therefore, reducing GNN complexity may not be a viable option for defending against GTA, as it may negatively impact system performance.

Q5: Why is GTA downstream model-agnostic?

We have shown in § 4 that the effectiveness of GTA seems agnostic to the downstream models. Here we provide a possible explanation for this phenomenon.

Let \tilde{G} be an arbitrary trigger-embedded graph. Recall that the optimization of Eq (5) essentially shifts \tilde{G} in the feature space by minimizing $\Delta_{f_\theta}(\tilde{G}) = \|f_\theta(\tilde{G}) - \mathbb{E}_{G \sim P_y} f_\theta(G)\|$ (with

respect to classes other than y_i), where P_{y_i} is the data distribution of target class y_i .

Now consider the end-to-end system $h \circ f_\theta$. Apparently, if $\Delta_{h \circ f_\theta}(\tilde{G}) = \|h \circ f_\theta(\tilde{G}) - \mathbb{E}_{G \sim P_{y_i}} h \circ f_\theta(G)\|$ is minimized (with respect to classes other than y_i), it is likely that \tilde{G} is classified as y_i . One sufficient condition is that $\Delta_{h \circ f_\theta}$ is linearly correlated with Δ_{f_θ} : $\Delta_{h \circ f_\theta} \propto \Delta_{f_\theta}$. If so, we say that the function represented by downstream model h is pseudo-linear [24].

Yet, compared with GNNs, most downstream models are fairly simple (e.g., one fully-connected layer) and tend to show strong pseudo-linearity, making GTA agnostic to downstream models. One may thus suggest mitigating GTA by adopting complex downstream models. However, the option may not be feasible: (i) complex models are difficult to train especially when the training data is limited, which is often the case in transfer learning; and (ii) the ground-truth mapping from the feature space to the output space may be indeed pseudo-linear, independent of downstream models.

Q6: Why is GTA difficult to defend against?

As GTA represents a new class of backdoor attacks, one possibility is to adopt existing mitigation in other domains (e.g., images) to defend against GTA. Below we evaluate the effectiveness of this strategy.

Detection design – We aim to detect suspicious GNNs and potential backdoors at the model inspection stage [8, 31, 56]. We consider NEURALCLEANSE [56] as a representative method, upon which we build our defense against GTA. Intuitively, given a DNN, NEURALCLEANSE searches for potential backdoors in every class. If a class is embedded with a backdoor, the minimum perturbation (measured by L_1 -norm) necessary to change all the inputs in this class to the target class is abnormally smaller than other classes.

To apply this defense in our context, we introduce the definition below. Given trigger g_t and to-be-replaced subgraph g , let g_t comprise nodes v_1, \dots, v_n and g correspondingly comprise u_1, \dots, u_n . The cost of substituting g with g_t is measured by the L_1 distance of their concatenated features:

$$\Delta(g_t, g) = \|X_{v_1} \uplus \dots \uplus X_{v_n} - X_{u_1} \uplus \dots \uplus X_{u_n}\|_1 \quad (12)$$

where X_{v_i} is v_i 's feature vector and \uplus denotes the concatenation operator. Intuitively, this measure accounts for both topology and feature perturbation.

We assume a set of benign graphs \mathcal{D} . Let \mathcal{D}_y be the subset of \mathcal{D} in class y and \mathcal{D}_y as the rest. For each class y , we search for the optimal trigger g_t to change the classification of all the graphs in \mathcal{D}_y to y . The optimality is defined in terms of the minimum perturbation cost (MPC):

$$\min_{g_t} \sum_{G \in \mathcal{D}_y} \min_{g \subset G} \Delta(g_t, g) \quad \text{s.t.} \quad h \circ f_\theta(G \ominus g \oplus g_t) = y \quad (13)$$

where $G \ominus g \oplus g_t$ denotes G after substituting g with g_t .

Recall that the variants of GTA assume different trigger definitions. Correspondingly, we consider three settings for searching for potential triggers: (i) the trigger g_t^I with topology and features universal for all the graphs in \mathcal{D}_y ; (ii) the trigger g_t^{II} with universal topology but features adapted to individual graphs; and (iii) the trigger g_t^{III} with both topology and features adapted to individual graphs.

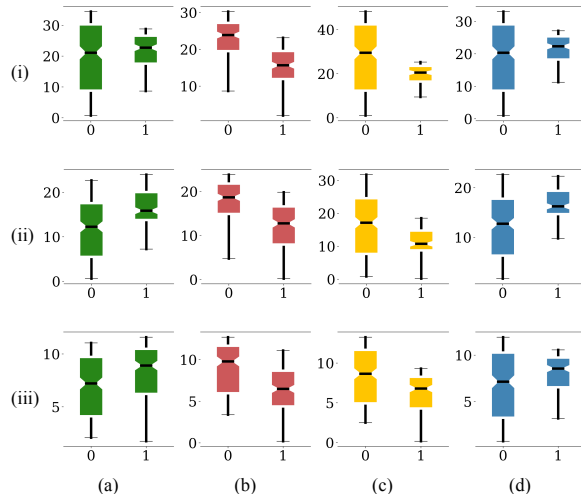


Figure 12: MPC-based backdoor detection (ChEMBL \rightarrow Toxicant): (i)-(iii) triggers with universal topology and features, universal topology and adaptive features, and adaptive topology and features; (a) benign GNN; (b)-(d) trojaned GNNs by GTA^I , GTA^{II} , and GTA^{III} .

Results and analysis – We evaluate the backdoor search method in the transfer case of pre-trained, off-the-shelf GNN models (ChemMBL \rightarrow Toxicant). We sample 100 graphs from each class ('0' and '1') of the Toxicant dataset to form \mathcal{D} . For comparison, we also run the search on a benign GNN model. All the attack variants consider '1' as the target class. Figure 12 visualizes the MPC measures with respect to each class under varying settings of GNN models, backdoor attacks, and trigger definitions.

We have the following observations. First, even on benign models, the MPC measure varies across the two classes, due to their inherent distributional heterogeneity. Second, on the same model (along each column), the measure decreases as the trigger definition becomes more adaptive because tailoring to individual graphs tends to lead to less perturbation. Third, most importantly, under the same trigger definition (along each row), GTA^I and GTA^{II} show significantly disparate MPC distributions across the two classes, while the MPC distributions of GTA^{III} and benign models seem fairly similar, implying the difficulty of distinguishing GNNs trojaned by GTA^{III} based on their MPC measures.

To quantitatively validate the above observations, on each model, we apply the one-tailed Kolmogorov-Smirnov test [42] between the MPC distributions of the two classes, with the null hypothesis being that the MPC of the target class is significantly lower than the other class (i.e., detectable). Table 8 summarizes the test results. Observe that regardless of the trigger definition, the trojaned models by GTA^I and GTA^{II}

show large p -values (≥ 0.08), thereby lacking support to reject the null hypothesis; meanwhile, the benign GNN and trojaned model by GTA^{III} demonstrate extremely small p -values (< 0.001), indicating strong evidence to reject the null hypothesis (i.e., the MPC of the target class is not significantly lower). Thus, relying on MPC to detect GTA^{III} tends to give missing or incorrect results. We also conduct additional statistical tests (e.g., class-wise comparison of benign and trojaned models), with details deferred to Appendix C.

Trigger Definition	p -Value of GNN under Inspection			
	Benign	GTA ^I	GTA ^{II}	GTA ^{III}
g_r^I	2.6×10^{-9}	1.0×10^{-0}	1.8×10^{-1}	5.4×10^{-7}
g_r^{II}	5.8×10^{-11}	1.0×10^{-0}	2.6×10^{-1}	1.3×10^{-13}
g_r^{III}	1.9×10^{-5}	1.7×10^{-1}	8.4×10^{-2}	9.3×10^{-4}

Table 8. Kolmogorov-Smirnov test of the MPC measures of benign and trojaned GNNs (ChEMBL \rightarrow Toxicant).

We now provide a possible explanation for the above observations. Intuitively, NEURALCLEANSE relies on the assumption that a trojaned model creates a “shortcut” (i.e., the trigger perturbation) for all the trigger-embedded inputs to reach the target class. However, this premise may not necessarily hold for GTA^{III}: because of its adaptive nature, each individual graph can have a specific shortcut to reach the target class, rendering the detection less effective. Thus, it seems crucial to carefully account for the trigger adaptiveness in designing effective countermeasures against GTA, which we consider as our ongoing research.

We have also evaluated the detectability of GTA under the transductive setting (with details in Appendix C), which leads to similar conclusions.

6 Related Work

With their widespread use in security-critical domains, DNNs are becoming the new targets of malicious manipulations [3]. Two primary types of attacks are considered in the literature: adversarial attacks and backdoor attacks.

Adversarial attacks – One line of work focuses on developing new attacks of crafting adversarial inputs to deceive target DNNs [6, 18, 41, 50]. The attacks can be classified as untargeted (i.e., the adversary desires to simply force misclassification) and targeted (i.e., the adversary desires to force the inputs to be misclassified into specific classes).

Another line of work attempts to improve DNN resilience against existing attacks by devising new training strategies (e.g., adversarial training) [20, 27, 40, 52] or detection methods [17, 33, 36, 64]. However, such defenses are often penetrated or circumvented by even stronger attacks [1, 29], resulting in a constant arms race.

Backdoor attacks – The existing backdoor attacks can be classified based on their targets. In class-level attacks, specific triggers (e.g., watermarks) are often pre-defined, while the adversary aims to force all the trigger-embedded inputs to be misclassified by the trojaned model [19, 32]. In instance-level

attacks (“clean-label” backdoors), the targets are defined as specific, unmodified inputs, while the adversary attempts to force such inputs to be misclassified by the trojaned model [24, 25, 47, 49].

The existing defenses against backdoor attacks mostly focus on class-level attacks, which, according to their strategies, include (i) cleansing potential contaminated data at training time [53], (ii) identifying suspicious models during model inspection [8, 31, 56], and (iii) detecting trigger-embedded inputs at inference time [7, 10, 13, 16].

Attacks against GNNs – In contrast of the intensive research on DNNs for continuous data (e.g., images), the studies on the security vulnerabilities of GNNs for graph-structured data are still sparse. One line of work attempts to deceive GNNs via perturbing the topological structures or descriptive features of graph data at inference time [12, 57, 68]. Another line of work aims to poison GNNs at training time to degrade their overall performance [4, 30, 69]. The defenses [58, 62] against such attacks are mostly inspired by that for general DNNs (e.g., adversarial training [34]).

Despite the plethora of prior work, thus far little is known about the vulnerabilities of GNN models to backdoor attacks. This work bridges this striking gap by designing, implementing, and evaluating the first backdoor attack on GNNs.

7 Conclusion

This work represents an in-depth study on the vulnerabilities of GNN models to backdoor attacks. We present GTA, the first attack that trojans GNNs and invokes malicious functions in downstream tasks via triggers tailored to individual graphs. Through extensive empirical evaluation using benchmark datasets and state-of-the-art models, we showcase the practicality of GTA in a range of security-critical applications, raising severe concerns about the current practice of re-using pre-trained GNNs. Moreover, we provide analytical justification for such vulnerabilities and discuss potential mitigation, which might shed light on pre-training and re-using GNNs in a more robust fashion.

This work also opens up several avenues for further investigation. First, while we focus on class-level backdoor attacks, it is equally important to understand the vulnerabilities of GNNs to instance-level backdoor attacks. Second, recent studies [39] have shown that adversarial inputs and trojaned DNNs mutually reinforce each other; it is worth studying whether such effects also exist for GNNs. Lastly, implementing and evaluating other existing mitigation against backdoor attacks in the context of GNNs may serve as a promising starting point for developing effective defenses against GTA.

References

- [1] Anish Athalye, Nicholas Carlini, and David Wagner. Obfuscated Gradients Give a False Sense of Security: Circumventing Defenses to Adversarial Examples. In *Proceedings of IEEE Conference on Machine Learning (ICML)*, 2018.
- [2] Battista Biggio, Giorgio Fumera, Fabio Roli, and Luca Didaci. Poisoning Adaptive Biometric Systems. In *Proceedings of Joint IAPR International Workshop on Structural, Syntactic, and Statistical Pattern Recognition (SSPR&SPR)*, 2012.
- [3] Battista Biggio and Fabio Roli. Wild Patterns: Ten Years after The Rise of Adversarial Machine Learning. *Pattern Recognition*, 84:317–331, 2018.
- [4] Aleksandar Bojchevski and Stephan Günnemann. Adversarial Attacks on Node Embeddings via Graph Poisoning. In *Proceedings of IEEE Conference on Machine Learning (ICML)*, 2019.
- [5] BVLC. ModelZoo. <https://github.com/BVLC/caffe/wiki/Model-Zoo>, 2017.
- [6] Nicholas Carlini and David A. Wagner. Towards Evaluating the Robustness of Neural Networks. In *Proceedings of IEEE Symposium on Security and Privacy (S&P)*, 2017.
- [7] Bryant Chen, Wilka Carvalho, Nathalie Baracaldo, Heiko Ludwig, Benjamin Edwards, Taesung Lee, Ian Molloy, and Biplav Srivastava. Detecting Backdoor Attacks on Deep Neural Networks by Activation Clustering. In *ArXiv e-prints*, 2018.
- [8] Huili Chen, Cheng Fu, Jishen Zhao, and Farinaz Koushanfar. DeepInspect: A Black-box Trojan Detection and Mitigation Framework for Deep Neural Networks. In *Proceedings of International Joint Conference on Artificial Intelligence*, 2019.
- [9] Xinyun Chen, Chang Liu, Bo Li, Kimberly Lu, and Dawn Song. Targeted Backdoor Attacks on Deep Learning Systems Using Data Poisoning. *ArXiv e-prints*, 2017.
- [10] Edward Chou, Florian Tramer, Giancarlo Pellegrino, and Dan Boneh. SentiNet: Detecting Physical Attacks Against Deep Learning Systems. In *ArXiv e-prints*, 2018.
- [11] Paul Cooper. Meet AISight: The scary CCTV network completely run by AI. <http://www.itproportal.com/>, 2014.
- [12] Hanjun Dai, Hui Li, Tian Tian, Xin Huang, Wang Lin, Jun Zhu, and Le Song. Adversarial Attack on Graph Structured Data. In *Proceedings of IEEE Conference on Machine Learning (ICML)*, 2018.
- [13] Bao Doan, Ehsan Abbasnejad, and Damith Ranasinghe. Februus: Input Purification Defense Against Trojan Attacks on Deep Neural Network Systems. In *ArXiv e-prints*, 2020.
- [14] Elliptic. www.elliptic.co.
- [15] Luca Franceschi, Paolo Frasconi, Saverio Salzo, Riccardo Grazi, and Massimiliano Pontil. Bilevel Programming for Hyperparameter Optimization and Meta-Learning. In *Proceedings of IEEE Conference on Machine Learning (ICML)*, 2018.
- [16] Yansong Gao, Chang Xu, Derui Wang, Shiping Chen, Damith Ranasinghe, and Surya Nepal. STRIP: A Defence Against Trojan Attacks on Deep Neural Networks. In *ArXiv e-prints*, 2019.
- [17] T. Gehr, M. Mirman, D. Drachler-Cohen, P. Tsankov, S. Chaudhuri, and M. Vechev. AI2: Safety and Robustness Certification of Neural Networks with Abstract Interpretation. In *Proceedings of IEEE Symposium on Security and Privacy (S&P)*, 2018.
- [18] Ian Goodfellow, Jonathon Shlens, and Christian Szegedy. Explaining and Harnessing Adversarial Examples. In *Proceedings of International Conference on Learning Representations (ICLR)*, 2015.
- [19] Tianyu Gu, Brendan Dolan-Gavitt, and Siddharth Garg. BadNets: Identifying Vulnerabilities in the Machine Learning Model Supply Chain. *ArXiv e-prints*, 2017.
- [20] Chuan Guo, Mayank Rana, Moustapha Cissé, and Laurens van der Maaten. Countering Adversarial Images Using Input Transformations. In *Proceedings of International Conference on Learning Representations (ICLR)*, 2018.
- [21] William L. Hamilton, Rex Ying, and Jure Leskovec. Inductive Representation Learning on Large Graphs. In *Proceedings of Advances in Neural Information Processing Systems (NeurIPS)*, 2017.
- [22] William L. Hamilton, Rex Ying, and Jure Leskovec. Representation Learning on Graphs: Methods and Applications. *IEEE Data Engineering Bulletin*, 3(40):52–74, 2017.
- [23] Weihua Hu, Bowen Liu, Joseph Gomes, Marinka Zitnik, Percy Liang, Vijay Pande, and Jure Leskovec. Strategies for Pre-training Graph Neural Networks. In *Proceedings of International Conference on Learning Representations (ICLR)*, 2020.
- [24] Yujie Ji, Xinyang Zhang, Shouling Ji, Xiapu Luo, and Ting Wang. Model-Reuse Attacks on Deep Learning Systems. In *Proceedings of ACM SAC Conference on Computer and Communications (CCS)*, 2018.
- [25] Yujie Ji, Xinyang Zhang, and Ting Wang. Backdoor Attacks against Learning Systems. In *Proceedings of IEEE Conference on Communications and Network Security (CNS)*, 2017.
- [26] Thomas N. Kipf and Max Welling. Semi-Supervised Classification with Graph Convolutional Networks. In *Proceedings of International Conference on Learning Representations (ICLR)*, 2017.
- [27] Alexey Kurakin, Ian J. Goodfellow, and Samy Bengio. Adversarial Machine Learning at Scale. In *Proceedings of International Conference on Learning Representations (ICLR)*, 2017.
- [28] Shaofeng Li, Benjamin Zi Hao Zhao, Jiahao Yu, Minhui Xue, Dali Kaafar, and Haojin Zhu. Invisible Backdoor Attacks Against Deep Neural Networks. *ArXiv e-prints*, 2019.
- [29] X. Ling, S. Ji, J. Zou, J. Wang, C. Wu, B. Li, and T. Wang. DEEPSEC: A Uniform Platform for Security Analysis of Deep Learning Model. In *Proceedings of IEEE Symposium on Security and Privacy (S&P)*, 2019.
- [30] Xuanqing Liu, Si Si, Xiaojin Zhu, Yang Li, and Cho-Jui Hsieh. A Unified Framework for Data Poisoning Attack to Graph-based Semi-supervised Learning. In *Proceedings of Advances in Neural Information Processing Systems (NeurIPS)*, 2019.

- [31] Yingqi Liu, Wen-Chuan Lee, Guanhong Tao, Shiqing Ma, Yousra Aafer, and Xiangyu Zhang. ABS: Scanning Neural Networks for Back-Doors by Artificial Brain Stimulation. In *Proceedings of ACM SAC Conference on Computer and Communications (CCS)*, 2019.
- [32] Yingqi Liu, Shiqing Ma, Yousra Aafer, Wen-Chuan Lee, Juan Zhai, Weihang Wang, and Xiangyu Zhang. Trojaning attack on neural networks. In *Proceedings of Network and Distributed System Security Symposium (NDSS)*, 2018.
- [33] Shiqing Ma, Yingqi Liu, Guanhong Tao, Wen-Chuan Lee, and Xiangyu Zhang. NIC: Detecting Adversarial Samples with Neural Network Invariant Checking. In *Proceedings of Network and Distributed System Security Symposium (NDSS)*, 2019.
- [34] Aleksander Madry, Aleksandar Makelov, Ludwig Schmidt, Dimitris Tsipras, and Adrian Vladu. Towards Deep Learning Models Resistant to Adversarial Attacks. In *Proceedings of International Conference on Learning Representations (ICLR)*, 2018.
- [35] Andreas Mayr, Günter Klambauer, Thomas Unterthiner, Marvin Steijaert, Jörg K. Wegner, Hugo Ceulemans, Djork-Arné Clevert, and Sepp Hochreiter. Large-Scale Comparison of Machine Learning Methods for Drug Target Prediction on ChEMBL. *Chem. Sci.*, 9:5441–5451, 2018.
- [36] Dongyu Meng and Hao Chen. MagNet: A Two-Pronged Defense Against Adversarial Examples. In *Proceedings of ACM SAC Conference on Computer and Communications (CCS)*, 2017.
- [37] Michel Neuhaus and Horst Bunke. A Graph Matching Based Approach to Fingerprint Classification Using Directional Variance. *Lecture Notes in Computer Science*, 3546:455–501, 2005.
- [38] Luigi P. Cordella, Pasquale Foggia, Carlo Sansone, and Mario Vento. A (Sub)Graph Isomorphism Algorithm for Matching Large Graphs. *IEEE Trans. Pattern Anal. Mach. Intell.*, 26(10):1367–1372, 2004.
- [39] Ren Pang, Hua Shen, Xinyang Zhang, Shouling Ji, Yevgeniy Vorobeychik, Xiapu Luo, Alex Liu, and Ting Wang. A Tale of Evil Twins: Adversarial Inputs versus Poisoned Models. In *Proceedings of ACM SAC Conference on Computer and Communications (CCS)*, 2020.
- [40] Nicolas Papernot, Patrick McDaniel, Xi Wu, Somesh Jha, and Ananthram Swami. Distillation as a Defense to Adversarial Perturbations Against Deep Neural Networks. In *Proceedings of IEEE Symposium on Security and Privacy (S&P)*, 2016.
- [41] Nicolas Papernot, Patrick D. McDaniel, Somesh Jha, Matt Fredrikson, Z. Berkay Celik, and Ananthram Swami. The Limitations of Deep Learning in Adversarial Settings. In *Proceedings of IEEE European Symposium on Security and Privacy (Euro S&P)*, 2016.
- [42] Dimitris N. Politis, Joseph P. Romano, and Michael Wolf. *Subsampling*. Springer, 1999.
- [43] Smita Ranveer and Swapnaja Hiray. Comparative Analysis of Feature Extraction Methods of Malware Detection. *International Journal of Computer Applications*, 120(5), 2015.
- [44] Ryan A. Rossi and Nesreen K. Ahmed. The Network Data Repository with Interactive Graph Analytics and Visualization. In *Proceedings of AAAI Conference on Artificial Intelligence (AAAI)*, 2015.
- [45] Benedek Rozemberczki, Carl Allen, and Rik Sarkar. Multi-scale Attributed Node Embedding. In *ArXiv e-prints*, 2019.
- [46] D. Sculley, Gary Holt, Daniel Golovin, Eugene Davydov, Todd Phillips, Dietmar Ebner, Vinay Chaudhary, Michael Young, Jean-Francois Crespo, and Dan Dennison. Hidden Technical Debt in Machine Learning Systems. In *Proceedings of Advances in Neural Information Processing Systems (NeurIPS)*, 2015.
- [47] Ali Shafahi, W. Ronny Huang, Mahyar Najibi, Octavian Suci, Christoph Studer, Tudor Dumitras, and Tom Goldstein. Poison Frogs! Targeted Clean-Label Poisoning Attacks on Neural Networks. In *Proceedings of Advances in Neural Information Processing Systems (NeurIPS)*, 2018.
- [48] Wei Song, Heng Yin, Chang Liu, and Dawn Song. DeepMem: Learning Graph Neural Network Models for Fast and Robust Memory Forensic Analysis. In *Proceedings of ACM SAC Conference on Computer and Communications (CCS)*, 2018.
- [49] Octavian Suci, Radu Mărginean, Yiğitcan Kaya, Hal Daumé, III, and Tudor Dumitras. When Does Machine Learning FAIL? Generalized Transferability for Evasion and Poisoning Attacks. In *Proceedings of USENIX Security Symposium (SEC)*, 2018.
- [50] Christian Szegedy, Wojciech Zaremba, Ilya Sutskever, Joan Bruna, Dumitru Erhan, Ian Goodfellow, and Rob Fergus. Intriguing Properties of Neural Networks. In *Proceedings of International Conference on Learning Representations (ICLR)*, 2014.
- [51] Tox21 Data Challenge. <https://tripod.nih.gov/tox21/>, 2014.
- [52] F. Tramèr, A. Kurakin, N. Papernot, I. Goodfellow, D. Boneh, and P. McDaniel. Ensemble Adversarial Training: Attacks and Defenses. In *Proceedings of International Conference on Learning Representations (ICLR)*, 2018.
- [53] Brandon Tran, Jerry Li, and Aleksander Madry. Spectral Signatures in Backdoor Attacks. In *Proceedings of Advances in Neural Information Processing Systems (NeurIPS)*, 2018.
- [54] Petar Veličković, Guillem Cucurull, Arantxa Casanova, Adriana Romero, Pietro Liò, and Yoshua Bengio. Graph Attention Networks. In *Proceedings of International Conference on Learning Representations (ICLR)*, 2018.
- [55] Allyson Versprille. Researchers Hack Into Driverless Car System, Take Control of Vehicle. <http://www.nationaldefensemagazine.org/>, 2015.
- [56] B. Wang, Y. Yao, S. Shan, H. Li, B. Viswanath, H. Zheng, and B. Y. Zhao. Neural Cleanse: Identifying and Mitigating Backdoor Attacks in Neural Networks. In *Proceedings of IEEE Symposium on Security and Privacy (S&P)*, 2019.
- [57] Binghui Wang and Neil Zhenqiang Gong. Attacking Graph-based Classification via Manipulating the Graph Structure. In *Proceedings of ACM SAC Conference on Computer and Communications (CCS)*, 2019.

- [58] Shen Wang, Zhengzhang Chen, Jingchao Ni, Xiao Yu, Zhichun Li, Haifeng Chen, and Philip S. Yu. Adversarial Defense Framework for Graph Neural Network. In *ArXiv e-prints*, 2019.
- [59] Shen Wang, Zhengzhang Chen, Xiao Yu, Ding Li, Jingchao Ni, Lu-An Tang, Jiaping Gui, Zhichun Li, Haifeng Chen, and Philip S. Yu. Heterogeneous Graph Matching Networks for Unknown Malware Detection. In *Proceedings of International Joint Conference on Artificial Intelligence (IJCAI)*, 2019.
- [60] C.I. Watson and C.L. Wilson. *NIST Special Database 4, Fingerprint Database*. National Institute of Standards and Technology, 1992.
- [61] B. Yu. Weisfeiler and A. A. Leman. Reduction of A Graph to A Canonical Form and An Algebra Arising during This Reduction. *Nauchno-Tekhnicheskaya Informatsia*, 2:12–16, 1968.
- [62] Kaidi Xu, Hongge Chen, Sijia Liu, Pin-Yu Chen, Tsui-Wei Weng, Mingyi Hong, and Xue Lin. Topology Attack and Defense for Graph Neural Networks: An Optimization Perspective. In *Proceedings of International Joint Conference on Artificial Intelligence (IJCAI)*, 2019.
- [63] Keyulu Xu, Weihua Hu, Jure Leskovec, and Stefanie Jegelka. How Powerful are Graph Neural Networks? In *Proceedings of International Conference on Learning Representations (ICLR)*, 2019.
- [64] W. Xu, D. Evans, and Y. Qi. Feature Squeezing: Detecting Adversarial Examples in Deep Neural Networks. In *Proceedings of Network and Distributed System Security Symposium (NDSS)*, 2018.
- [65] Yuanshun Yao, Huiying Li, Haitao Zheng, and Ben Y. Zhao. Latent Backdoor Attacks on Deep Neural Networks. In *Proceedings of ACM SAC Conference on Computer and Communications (CCS)*, 2019.
- [66] Rex Ying, Jiaxuan You, Christopher Morris, Xiang Ren, William L. Hamilton, and Jure Leskovec. Hierarchical Graph Representation Learning with Differentiable Pooling. In *Proceedings of Advances in Neural Information Processing Systems (NeurIPS)*, 2018.
- [67] Jason Yosinski, Jeff Clune, Yoshua Bengio, and Hod Lipson. How Transferable Are Features in Deep Neural Networks? In *Proceedings of Advances in Neural Information Processing Systems (NeurIPS)*, 2014.
- [68] Daniel Zügner, Amir Akbarnejad, and Stephan Günnemann. Adversarial Attacks on Neural Networks for Graph Data. In *Proceedings of ACM International Conference on Knowledge Discovery and Data Mining (KDD)*, 2018.
- [69] Daniel Zügner and Stephan Günnemann. Adversarial Attacks on Graph Neural Networks via Meta Learning. In *Proceedings of International Conference on Learning Representations (ICLR)*, 2019.

Appendix

A: Implementation of look-ahead

Here we provide details of evaluating Eq (7). Applying the chain rule to Eq (7), we have the following result:

$$\nabla_{g_t} \ell_{\text{atk}}(\theta', g_t) - \xi \nabla_{g_t, \theta}^2 \ell_{\text{ret}}(\theta, g_t) \nabla_{\theta'} \ell_{\text{atk}}(\theta', g_t) \quad (14)$$

where $\theta' = \theta - \xi \nabla_{\theta} \ell_{\text{ret}}(\theta, g_t)$ is the updated parameter after the one-step look-ahead. Note that the formulation here involves a matrix-vector product, which can be approximated with the finite difference approximation. Let $\theta^{\pm} = \theta \pm \epsilon \nabla_{\theta'} \ell_{\text{atk}}(\theta', g_t)$ where ϵ is a small constant ($\epsilon = 10^{-5}$). Then we can approximate the second term in Eq (14) as:

$$\frac{\nabla_{g_t} \ell_{\text{ret}}(\theta^+, g_t) - \nabla_{g_t} \ell_{\text{ret}}(\theta^-, g_t)}{2\epsilon} \quad (15)$$

B: Default parameter setting

Table 9 summarizes the default parameter setting in § 4.

Type	Parameter	Setting
GCN	Architecture	2AL
GRAPHSAGE	Architecture	2AL
	Aggregator	Mean [21]
GCN (off-the-shelf)	Architecture	5AL
GAT	# Heads	3
Classifier	Architecture	1FC+1SM
Training	Optimizer	Adam
	Learning rate	0.01
	Weight decay	5e-4
	Dropout	0.5
	Epochs	50 (I), 100 (T)
	Batch size	32 (I)
Attack	n_{trigger}	3 (I), 6 (T)
	n_{io}	1
	n_{mask}	100% (I), 10% (T)
Trigger Generator	Optimizer	Adam
	Learning rate	0.01
	Epochs	20
Detection	# Samples	100 per class
	Significance level α	0.05
	λ_{ASR}	80%

Table 9. Default parameter setting. I: inductive, T: transductive, AL: aggregation layer, FC: fully-connected layer, SM: softmax layer.

C: Additional experiments

Here we list the results of additional experiments, which complement § 4 and § 5.

Class-wise MPC comparison (ChEMBL \rightarrow Toxicant) – We conduct the Student’s t -test on the class-wise MPC distributions of benign and trojaned GNNs in the transfer case of ChemMBL \rightarrow Toxicant, with the null hypothesis being that the two distributions are identical. The results are summarized in Table 10. Regardless of the trigger definition, GTA^I and GTA^{II}

feature small p -values ($\ll 0.05$), indicating strong evidence to reject the null hypothesis; that is, their MPC distributions significantly differ from the benign models. Meanwhile, GTA^{III} has larger p -values, thereby lacking of support to reject the null hypothesis; that is, the MPC distributions of benign and trojaned models by GTA^{III} are not distinguishable, implying the challenge of detecting GTA^{III} based on its MPC distributions. The results here complement Table 8.

Trigger	GNNs	p -Value of GNN under Inspection	
		label 0	label 1
g_r^I	GTA^I	3.0×10^{-15}	1.4×10^{-41}
	GTA^{II}	4.8×10^{-12}	1.6×10^{-5}
	GTA^{III}	1.4×10^{-1}	6.7×10^{-2}
g_r^{II}	GTA^I	1.6×10^{-31}	5.5×10^{-26}
	GTA^{II}	1.0×10^{-12}	7.6×10^{-8}
	GTA^{III}	3.1×10^{-2}	4.6×10^{-2}
g_r^{III}	GTA^I	7.5×10^{-6}	8.4×10^{-19}
	GTA^{II}	6.2×10^{-8}	1.2×10^{-5}
	GTA^{III}	1.1×10^{-2}	3.5×10^{-1}

Table 10. Student’s t -test on the class-wise MPC measures of benign and trojaned GNNs (ChEMBL \rightarrow Toxicant).

MPC-based backdoor detection (Toxicant \rightarrow AIDS) –

We also apply the backdoor detection on the transfer case of Toxicant \rightarrow AIDS, with results shown in Figure 13, Table 11, and Table 12, which show trends similar to the case of Toxicant \rightarrow AIDS in § 5, indicating the challenge of detecting GTA^{III} on pre-trained GNN models.

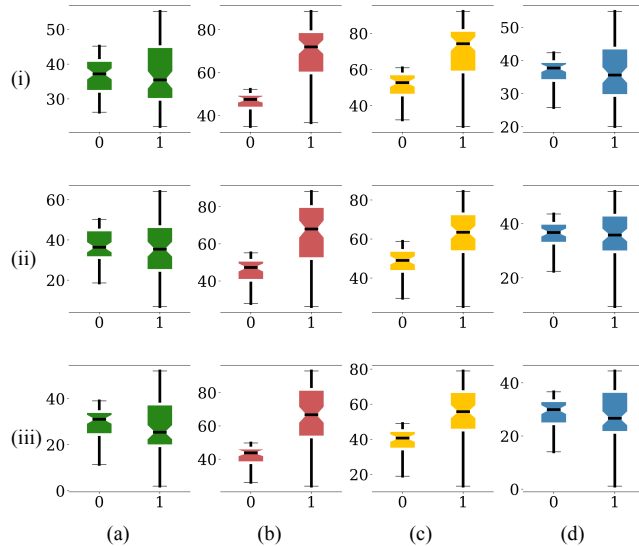


Figure 13: MPC-based backdoor detection (Toxicant \rightarrow AIDS).

Trigger Definition	p -Value of GNN under Inspection			
	Benign	GTA^I	GTA^{II}	GTA^{III}
g_r^I	2.7×10^{-2}	1.0×10^{-0}	9.1×10^{-1}	3.9×10^{-2}
g_r^{II}	3.1×10^{-3}	1.0×10^{-0}	6.1×10^{-1}	1.8×10^{-2}
g_r^{III}	3.1×10^{-3}	9.6×10^{-1}	8.5×10^{-1}	7.8×10^{-3}

Table 11. Kolmogorov-Smirnov test on the MPC of benign and trojaned GNNs (Toxicant \rightarrow AIDS).

MPC-based backdoor detection (Bitcoin) – We evaluate the detectability of GTA under the transductive setting. Specif-

Trigger Definition	GNN	p -Value of GNN under Inspection	
		Class 0	Class 1
g_r^I	GTA^I	3.5×10^{-28}	5.2×10^{-51}
	GTA^{II}	6.1×10^{-39}	5.0×10^{-41}
	GTA^{III}	2.1×10^{-1}	4.6×10^{-2}
g_r^{II}	GTA^I	2.9×10^{-12}	2.8×10^{-29}
	GTA^{II}	1.7×10^{-16}	6.2×10^{-21}
	GTA^{III}	3.8×10^{-2}	4.4×10^{-2}
g_r^{III}	GTA^I	6.0×10^{-16}	2.7×10^{-24}
	GTA^{II}	3.9×10^{-18}	4.6×10^{-31}
	GTA^{III}	2.9×10^{-1}	5.6×10^{-2}

Table 12. Student’s t -test on the class-wise MPC measures of benign and trojaned GNNs (Toxicant \rightarrow AIDS).

ically, we search for a minimal trigger g_r that, if replacing a subgraph g randomly sampled from the given graph G , results in large ASR (misclassification of unlabeled nodes within K hops of g). In implementation, we set a threshold λ_{ASR} (Table 9). A trigger g_r is considered as a candidate if it attains λ_{ASR} over 10 randomly sampled subgraphs (of the same size as g_r) from G . We then pick the candidate with the minimum MPC as defined in Eq (13) as the detected trigger.

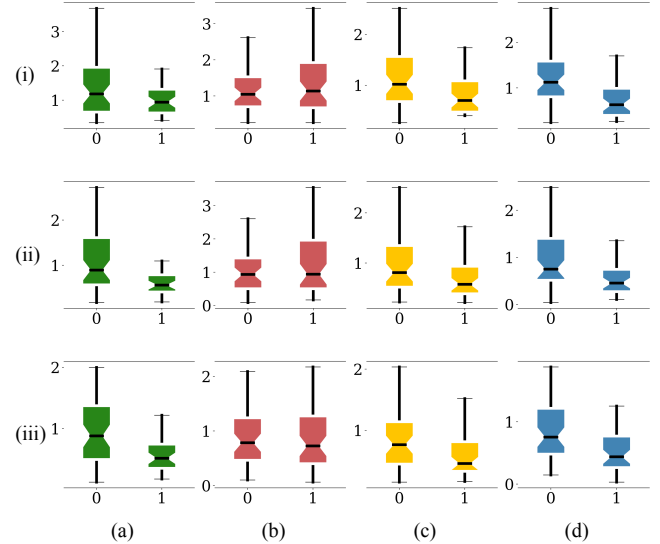


Figure 14: MPC-based backdoor detection (Bitcoin).

Trigger Definition	p -Value of GNN under Inspection			
	Benign	GTA^I	GTA^{II}	GTA^{III}
g_r^I	9.1×10^{-3}	7.6×10^{-1}	3.8×10^{-2}	9.6×10^{-5}
g_r^{II}	2.8×10^{-4}	5.5×10^{-1}	7.9×10^{-3}	2.3×10^{-3}
g_r^{III}	2.8×10^{-4}	4.4×10^{-1}	5.9×10^{-4}	4.3×10^{-3}

Table 13. Kolmogorov-Smirnov test on the MPC measures of benign and trojaned GNNs (Bitcoin).

Figure 14 summarizes the MPC measures with respect to each class under varying settings of GNNs, backdoor attacks, and trigger definitions. Note that the benign and trojaned models by GTA^{II} and GTA^{III} show similar MPC distributions, different from GTA^I . Table 13 further quantitatively validates this observation. We apply one-sided Kolmogorov-Smirnov test on the MPC distributions between the two classes on each model, with the null hypothesis being that the MPC of the target class (‘0’) is significantly lower than the other class.

Observe that except for GTA¹, the other three models show fairly small p -values (< 0.04), indicating strong evidence to reject the null hypothesis. Thus, relying on MPC to detect GTA tends to result in missing or incorrect results.

More samples of trigger-embedded graphs – Figure 15 shows sample graphs and their trigger-embedded counterparts under the transductive setting.

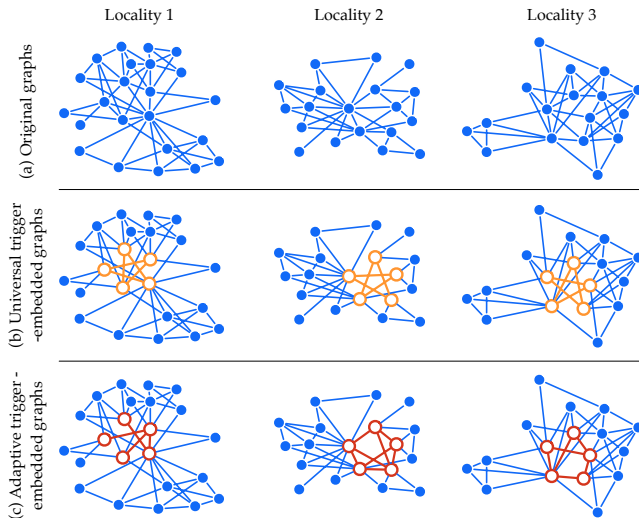


Figure 15: Illustration of backdoor attacks on social networks from the Facebook dataset [45]: (a) original graphs; (b) universal trigger-embedded graphs; (c) adaptive trigger-embedded graphs.